JACC: CARDIOVASCULAR IMAGING VOL. ■, NO. ■, 2018

PUBLISHED BY ELSEVIER

Identification of High-Risk Plaques Destined to Cause Acute Coronary Syndrome Using Coronary Computed Tomographic Angiography and Computational Fluid Dynamics

Joo Myung Lee, MD, MPH, PhD,[a] Gilwoo Choi, PhD,[b] Bon-Kwon Koo, MD, PhD,[c,d] Doyeon Hwang, MD,[c] Jonghanne Park, MD, PhD,[c] Jinlong Zhang, MD,[c] Kyung-Jin Kim, MD,[c] Yaliang Tong, MD,[e] Hyun Jin Kim, PhD,[b] Leo Grady, PhD,[b] Joon-Hyung Doh, MD, PhD,[f] Chang-Wook Nam, MD, PhD,[g] Eun-Seok Shin, MD, PhD,[h] Young-Seok Cho, MD, PhD,[i] Su-Yeon Choi, MD, PhD,[j] Eun Ju Chun, MD, PhD,[k] Jin-Ho Choi, MD, PhD,[a] Bjarne L. Nørgaard, MD, PhD,[l] Evald Christiansen, MD, PhD,[l] Koen Niemen, MD, PhD,[m,n] Hiromasa Otake, MD, PhD,[o] Martin Penicka, MD, PhD,[p] Bernard de Bruyne, MD, PhD,[p] Takashi Kubo, MD, PhD,[q] Takashi Akasaka, MD, PhD,[q] Jagat Narula, MD, PhD,[r] Pamela S. Douglas, MD,[s] Charles A. Taylor, PhD,[b,t] Hyo-Soo Kim, MD, PhD[c]

ABSTRACT

OBJECTIVES We investigated the utility of noninvasive hemodynamic assessment in the identification of high-risk plaques that caused subsequent acute coronary syndrome (ACS).

BACKGROUND ACS is a critical event that impacts the prognosis of patients with coronary artery disease. However, the role of hemodynamic factors in the development of ACS is not well-known.

METHODS Seventy-two patients with clearly documented ACS and available coronary computed tomographic angiography (CTA) acquired between 1 month and 2 years before the development of ACS were included. In 66 culprit and 150 nonculprit lesions as a case-control design, the presence of adverse plaque characteristics (APC) was assessed and hemodynamic parameters (fractional flow reserve derived by coronary computed tomographic angiography [FFR_{CT}], change in FFR_{CT} across the lesion [$\triangle FFR_{CT}$], wall shear stress [WSS], and axial plaque stress) were analyzed using computational fluid dynamics. The best cut-off values for FFR_{CT}, $\triangle FFR_{CT}$, WSS, and axial plaque stress were used to define the presence of adverse hemodynamic characteristics (AHC). The incremental discriminant and reclassification abilities for ACS prediction were compared among 3 models (model 1: percent diameter stenosis [%DS] and lesion length, model 2: model 1 + APC, and model 3: model 2 + AHC).

RESULTS The culprit lesions showed higher %DS (55.5 ± 15.4% vs. 43.1 ± 15.0%; $p < 0.001$) and higher prevalence of APC (80.3% vs. 42.0%; $p < 0.001$) than nonculprit lesions. Regarding hemodynamic parameters, culprit lesions showed lower FFR_{CT} and higher $\triangle FFR_{CT}$, WSS, and axial plaque stress than nonculprit lesions (all p values <0.01). Among the 3 models, model 3, which included hemodynamic parameters, showed the highest c-index, and better discrimination (concordance statistic [c-index] 0.789 vs. 0.747; $p = 0.014$) and reclassification abilities (category-free net reclassification index 0.287; $p = 0.047$; relative integrated discrimination improvement 0.368; $p < 0.001$) than model 2. Lesions with both APC and AHC showed significantly higher risk of the culprit for subsequent ACS than those with no APC/AHC (hazard ratio: 11.75; 95% confidence interval: 2.85 to 48.51; $p = 0.001$) and with either APC or AHC (hazard ratio: 3.22; 95% confidence interval: 1.86 to 5.55; $p < 0.001$).

CONCLUSIONS Noninvasive hemodynamic assessment enhanced the identification of high-risk plaques that subsequently caused ACS. The integration of noninvasive hemodynamic assessments may improve the identification of culprit lesions for future ACS. (Exploring the Mechanism of Plaque Rupture in Acute Coronary Syndrome Using Coronary CT Angiography and Computational Fluid Dynamic [EMERALD]; NCT02374775) (J Am Coll Cardiol Img 2018;■:■-■)

ISSN 1936-878X/$36.00 https://doi.org/10.1016/j.jcmg.2018.01.023

ABBREVIATIONS AND ACRONYMS

ACS = acute coronary syndrome

AUC = area under curve

CI = confidence interval

CTA = computed tomography angiography

DS = diameter stenosis

FFR_{CT} = per-vessel fractional flow reserve derived from coronary computed tomography angiography

$\triangle FFR_{CT}$ = change in FFR_{CT} across the lesion

HR = hazard ratio

WSS = wall shear stress

Acute coronary syndrome (ACS) and sudden cardiac death can be the first manifestation of coronary artery disease and are the leading causes of death in the majority of the world's population. The main pathophysiology of ACS is well-known and fibrous cap thickness, presence of a lipid core, and the degree of inflammation have been proposed as key determinants of plaque vulnerability (1). Previous studies using virtual histology intravascular ultrasound or optical coherence tomography showed that clinical application of this concept improved the prediction of ACS risk (2). However, these approaches have not been widely adopted in daily practice due to relatively low positive predictive values, low prevalence of high-risk plaques, unclear cost-effectiveness, and the invasive nature of diagnostic modalities (1).

Noninvasive imaging studies with coronary computed tomography angiography (CTA) also show the clinical value of coronary CTA-derived adverse plaque characteristics (APC) (3,4). In addition, the recent progress in coronary CTA and computational fluid dynamics (CFD) technologies enables simultaneous assessment of anatomical lesion severity, presence of APC, and quantification of hemodynamic forces acting on plaques in patient-specific geometric models (5-7). Because plaque rupture is a complicated biomechanical process influenced by the structure and constituents of the plaque as well as the external mechanical and hemodynamic forces acting on the plaque (8), a comprehensive evaluation of lesion geometry, plaque characteristics, and hemodynamic parameters may enhance the identification of high-risk plaque and the prediction of ACS risk.

The EMERALD (Exploring the MEchanism of plaque Rupture in Acute coronary syndrome using coronary CT Angiography and computationaL fluid Dynamics) study was conducted to evaluate the potential utility of comprehensive noninvasive hemodynamic assessment using coronary CTA and CFD in the identification of high-risk plaques that caused subsequent ACS.

METHODS

Detailed statistical methods are presented in the Online Appendix.

STUDY POPULATIONS. The study population was retrospectively enrolled from 11 international cardiovascular centers in 5 countries. Patients who suffered a clearly documented ACS (acute myocardial infarction [MI] or unstable angina with objective evidence of plaque rupture) and had undergone coronary CTA from 1 month to 2 years before the ACS event were enrolled (**Figures 1 and 2**). Acute MI was defined according to the universal definition of MI (9). All patients underwent invasive coronary angiography at the time of the ACS event. Patients with in-stent restenosis lesion-related ACS, secondary MI due to other general medical conditions, previous

From the [a]Department of Internal Medicine and Cardiovascular Center, Samsung Medical Center, Sungkyunkwan University School of Medicine, Seoul, Republic of Korea; [b]HeartFlow, Inc., Redwood City, California; [c]Department of Medicine, Seoul National University Hospital, Seoul, South Korea; [d]Institute on Aging, Seoul National University, Seoul, Korea; [e]Department of Cardiology, China-Japan Union Hospital of Jilin University, Changchun, China; [f]Department of Medicine, Inje University Ilsan Paik Hospital, Goyang, South Korea; [g]Department of Medicine, Keimyung University Dongsan Medical Center, Daegu, South Korea; [h]Department of Cardiology, Ulsan University Hospital, University of Ulsan College of Medicine, Ulsan, South Korea; [i]Department of Medicine, Seoul National University Bundang Hospital, Seongnam, South Korea; [j]Department of Internal Medicine, Seoul National University Healthcare System Gangnam Center, Seoul National University College of Medicine, Seoul, South Korea; [k]Department of Radiology, Seoul National University Bundang Hospital, Seongnam, South Korea; [l]Department of Cardiology, Aarhus University Hospital, Aarhus, Denmark; [m]Erasmus University Medical Center, Rotterdam, the Netherlands; [n]Cardiovascular Institute, Stanford University, School of Medicine, Stanford, California; [o]Department of Internal Medicine, Division of Cardiovascular and Respiratory Medicine, Kobe University Graduate School of Medicine, Kobe, Japan; [p]Cardiovascular Center Aalst, OLV-Clinic, Aalst, Belgium; [q]Department of Cardiovascular Medicine, Wakayama Medical University, Wakayama, Japan; [r]Icahn School of Medicine at Mount Sinai Hospital, New York, New York; [s]Duke Clinical Research Institute, Duke University School of Medicine, Durham, North Carolina; and the [t]Department of Bioengineering, Stanford University, Stanford, California. This study was funded by HeartFlow Inc. The company performed the computational fluid dynamics analysis, but had no role in study design, conduct, or manuscript preparation. Drs. G. Choi, H.J. Kim, Grady, and Taylor are employees and shareholders of HeartFlow, Inc., which provides the FFR_{CT} service. Dr. Douglas has received research grants from HeartFlow, Inc. and GE Healthcare. Dr. Nørgaard has received institutional unrestricted research grants from Siemens and HeartFlow, Inc. Dr. De Bruyne has received institutional unrestricted research grants from Abbott, Boston Scientific, Biotronik, and St. Jude Medical; has received consulting fees from St. Jude Medical, Opsens, and Boston Scientific; and is a shareholder for Siemens, GE, Bayer, Philips, HeartFlow, Inc., Edwards Life Sciences, Sanofi, and Omega Pharma. Dr. Niemen has received support from HeartFlow Inc., Siemens Healthineers, and GE Healthcare. Todd Villines, MD, served as the Guest Editor for this paper. Drs. Joo Myung Lee and Gilwoo Choi contributed equally to this work and are joint first authors.

Manuscript received October 15, 2017; revised manuscript received January 8, 2018, accepted January 9, 2018.

FIGURE 1 Study Flow

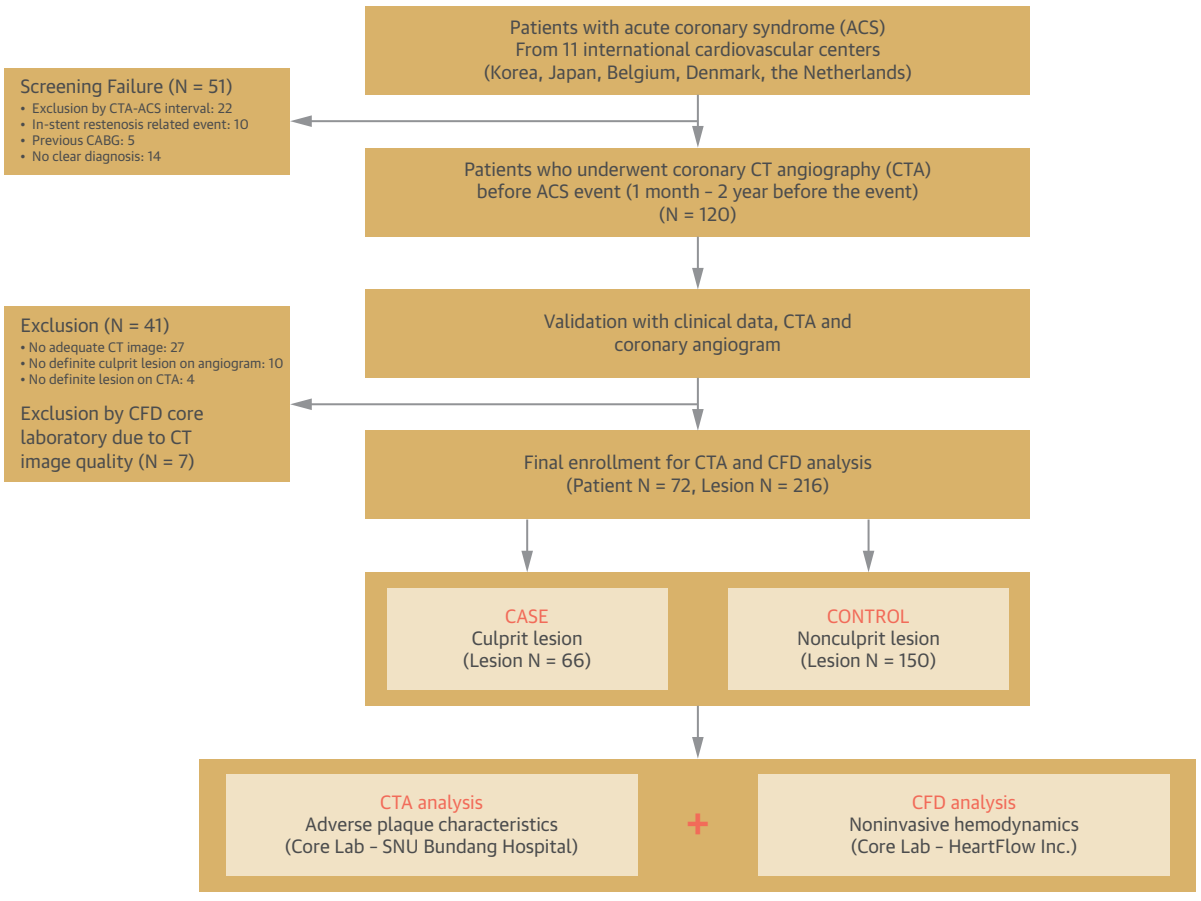

Patients presented with ACS who had undergone coronary CTA from 1 month to 2 years before the ACS event were enrolled. After screening of enrollment criteria and image quality, 72 patients (216 lesions) were finally analyzed. ACS = acute coronary syndrome; CABG = coronary artery bypass grafting; CFD = computational fluid dynamics; CT = computed tomography; CTA = computed tomographic angiography.

history of coronary artery bypass graft surgery, or inadequate image quality of coronary CTA for CFD analysis were excluded. The study protocol was approved by the institutional review board of each site and was conducted in accordance with the Declaration of Helsinki (NCT02374775).

ANALYSIS OF CORONARY CTA AND INVASIVE CORONARY ANGIOGRAPHY RESULTS. Coronary CTA images were screened for APC and CFD analyses at core laboratories in Seoul National University Bundang Hospital and HeartFlow, Inc., respectively (Online Figure 1). Lesions with diameter stenosis (DS) > 30% based on coronary CTA evaluation were included for subsequent APC analysis. The presence of APC (low-attenuation plaque, positive remodeling, napkin-ring sign, and spotty calcification) was assessed in each lesion by an independent observer blinded to the clinical data and CFD results according to the definitions from previous studies (3,4,7). Briefly, plaque density was assessed semi-automatically using a dedicated cardiac workstation (Intellispace Portal, Philips Healthcare, Eindhoven, the Netherlands) (7). Lesions were classified according to individual APC: low-attenuation plaque (average density ≤30 Hounsfield units [HU]), positive remodeling (lesion diameter/reference diameter ≥1.1), spotty calcification (average density >130 HU and diameter <3 mm), and napkin-ring sign (ring-like attenuation pattern with peripheral high attenuation tissue surrounding a central lower attenuation portion) (7).

FIGURE 2 Representative Case

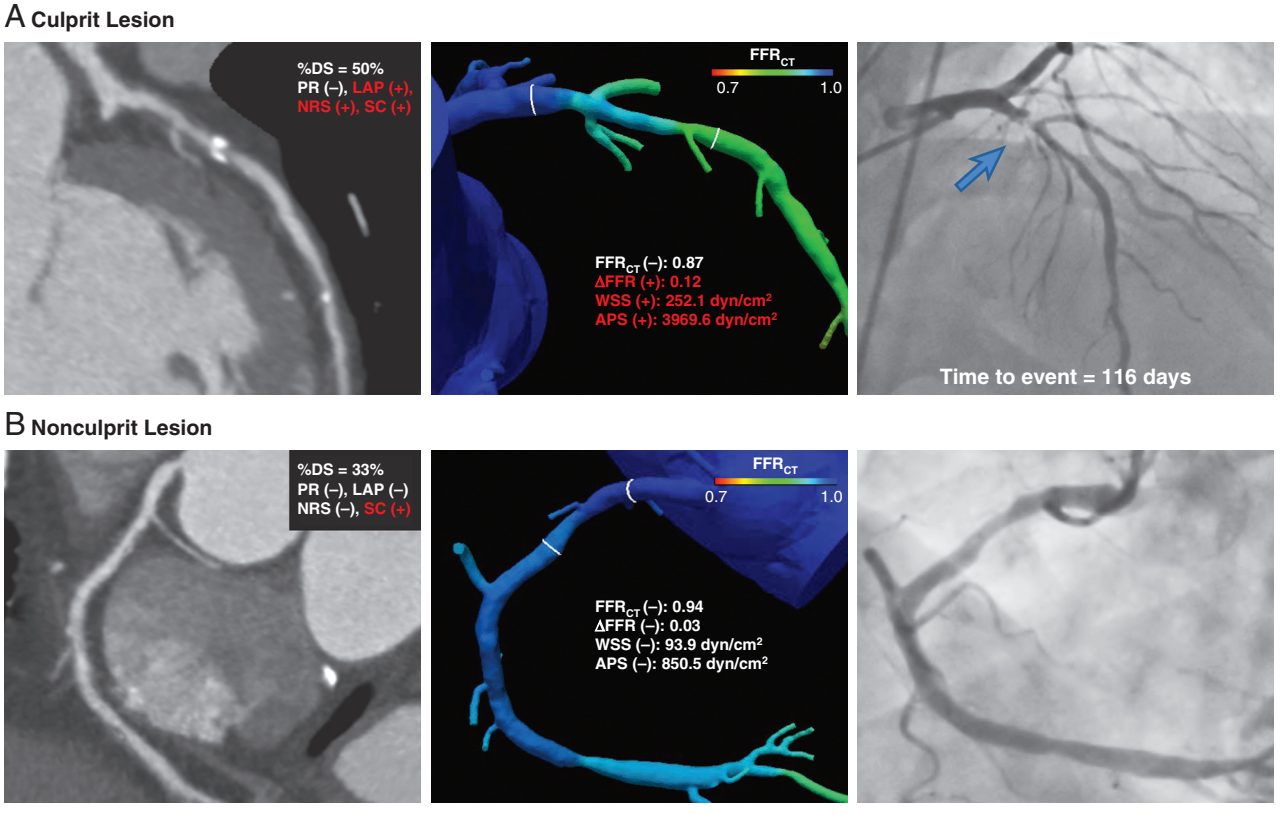

The patient had acute myocardial infarction 116 days after coronary computed tomographic angiography. **(A)** The culprit lesion in left anterior descending coronary artery had both adverse hemodynamic characteristics and adverse plaque characteristics, and **(B)** the nonculprit lesion in right coronary artery had only adverse plaque characteristics. APS = axial plaque stress; DS = percent diameter stenosis; FFR_{CT} = per-vessel fractional flow reserve derived from coronary computed tomographic angiography; $\triangle FFR_{CT}$ = change in FFR_{CT} across the lesion; LAP = low-attenuating plaque; NRS = napkin-ring sign; PR = positive remodeling; SC = spotty calcification; WSS = wall shear stress; other abbreviation as in Figure 1.

All angiograms were reviewed at a core laboratory (Seoul National University Hospital) and the culprit lesions were determined in a blinded fashion.

ANALYSIS OF HEMODYNAMIC PARAMETERS BY CFD. CFD was used to evaluate hemodynamic forces acting on coronary plaques. All CFD analyses were performed in a blinded fashion using the same procedure performed during per-vessel fractional flow reserve derived from coronary computed tomography angiography (FFR_{CT}) computation (Online Figure 1) (5-7). Briefly, coronary models, including all epicardial coronary arteries, were constructed by the extraction of vessel centerlines, identification of coronary plaques, and segmentation of lumen boundary along the coronary trees. Flow and pressure in the coronary model were computed by solving the Navier-Stokes equations, using CFD methods with assumptions of a rigid wall and a Newtonian fluid (6). Boundary conditions for hyperemia were derived from myocardial mass, vessel sizes at each outlet, and the response of the microcirculation to adenosine (5).

In consideration of potential clinical implications proposed in previous studies (6,7,10) 4 hemodynamic parameters were computed for covariates in prediction models: 1) FFR_{CT}; 2) change in FFR_{CT} across the lesion ($\triangle FFR_{CT}$); 3) wall shear stress (WSS) (7,11); and 4) axial plaque stress (6,10). Each hemodynamic parameter was computed at lesion locations defined during APC analysis, and was defined as follows (Online Figure 2). First, FFR_{CT} was defined by the ratio of mean downstream coronary pressure (Pd) and the aortic pressure (Pa) derived from the CFD analysis under a simulated hyperemic condition. Second, $\triangle FFR_{CT}$ was defined for each lesion by computing

the difference between the proximal and distal FFR_{CT} values as follows (Online Figure 2A):

$$\triangle FFR_{CT} = proximal\ FFR_{CT} - distal\ FFR_{CT}$$

Third, ($\overrightarrow{WSS}$) is the tangential stress resulting from the friction between blood flow and the endothelial surface of the vessel wall, and was computed by:

$$\overrightarrow{WSS} = \vec{t} - (\vec{t} \cdot \vec{n})\vec{n},$$

where $\vec{n}$ is the normal vector on the luminal surface of the blood vessel. Fourth, axial plaque stress is the axial component of the traction vector and was computed by:

$$\overrightarrow{Axial\ plaque\ stress} = (\vec{t} \cdot \vec{c})\vec{c},$$

where $\vec{t} \cdot \vec{c}$ is the dot product of the traction vector ($\vec{t}$) and tangential vector of vessel centerline ($\vec{c}$). For statistical analysis per lesion, WSS and axial plaque stress was averaged over the surface of the defined lesions as follows:

$$WSS_{lesion} = \frac{1}{A}\int_{X}^{Y} \|\overrightarrow{WSS}\| dA \text{ and}$$

$$|Axial\ Plaque\ Stress_{lesion}| = \left|\frac{1}{A}\int_{X}^{Y} (\vec{t} \cdot \vec{c}) dA,\right|$$

where A represents the surface area of a defined lesion from start (X) and end (Y) points (Online Figure 2B and 2C).

STATISTICAL ANALYSIS. All statistical analyses were performed on a per-lesion basis to compare culprit and nonculprit lesion characteristics. A generalized estimating equation was used to adjust intrasubject variability among vessels from the same patient. Continuous hemodynamic parameters were converted to binary variables by optimal cut-off values (FFR_{CT}: 0.80, $\triangle FFR_{CT}$: 0.06, WSS: 154.7 dyn/cm^2, and axial plaque stress: 1,606.6 dyn/cm^2) determined by receiver operating characteristics curve analysis (Online Figure 3). To evaluate the relative contribution of APC and hemodynamic parameters to the occurrence of ACS, lesions were classified according to the presence of APC and/or adverse hemodynamic characteristics (AHC). AHC was defined as lesions that have low FFR_{CT} (≤0.80), high $\triangle FFR_{CT}$ (≥0.06), high WSS (≥154.7 dyn/cm^2), or high axial plaque stress (≥1,606.6 dyn/cm^2).

Three prediction models were constructed to determine the incremental discriminatory and reclassification performance of hemodynamic parameters in identifying culprit lesions associated with subsequent ACS. As a baseline, an anatomy-based model (model 1) was derived from %DS and lesion length. The %DS was incorporated in model 1 as a categorical variable with classification of mild, moderate, or severe, according to <50%, 50% to 70%, and >70% DS, respectively. The lesion length was also converted into a binary variable using the best cut-off value of lesion length (≥12.5 mm vs. <12.5 mm). Then, an anatomy- and APC-based model (model 2) was derived from %DS, lesion length, and APC (i.e., model 1 + APC). As the last model including hemodynamic parameters, model 3 was derived from %DS, lesion length, APC and AHC set (i.e., model 2 + AHC). The discriminatory ability of model 3 was assessed by the Harrell's concordance statistic (c-index) and the

TABLE 1 Characteristics of the Patients and Lesions

Patients (n = 72)	
Age, yrs	69.9 ± 12.7
Male	54 (75.0)
Median interval between coronary CTA and acute coronary syndrome, days	338.0 (161.5-535.0)
Cardiovascular risk factors	
Hypertension	46 (63.9)
Diabetes mellitus	37 (51.4)
Hypercholesterolemia	35 (48.6)
Current smoker	22 (30.6)
Previous myocardial infarction	5 (6.9)
Ejection fraction, %	58.6 (44.5-63.3)
Clinical presentation	
Myocardial infarction	67 (93.0)
NSTEMI	41 (56.9)
STEMI	26 (36.1)
Unstable angina	5 (6.9)
Lesion characteristics (n = 216)	
Location	
Left main to LAD	87 (40.3)
LCX	48 (22.2)
RCA	81 (37.5)
Culprit vessel (n = 66)	
Left main to LAD	39 (59.1)
LCX	9 (13.6)
RCA	18 (27.3)
Characteristics	
Minimal lumen area, mm^2	2.75 ± 1.59
Diameter stenosis, %	46.9 ± 16.1
Distance from coronary ostium to MLA, mm	47.1 ± 22.6
Lesion length, mm	17.6 ± 7.4
FFR_{CT}	0.77 ± 0.15
FFR_{CT} ≤ 0.80	105 (48.6)

Values are mean ± SD, n (%), or median (25th and 75th percentile).

CTA = computed tomography angiography; FFR_{CT} = coronary computed tomographic angiography-derived fractional flow reserve; LAD = left anterior descending coronary artery; LCX = left circumflex artery; MLA = minimal lumen area; NSTEMI = non-ST-segment elevation myocardial infarction; RCA = right coronary artery; STEMI = ST-segment elevation myocardial infarction.

TABLE 2 Comparison of Lesion Characteristics, Adverse Plaque Characteristics, and Hemodynamic Parameters Between Culprit and Nonculprit Lesions

	Nonculprit Lesion (N = 150)	Culprit Lesion (N = 66)	p Value
Vessel location			0.001
LAD	48 (32.0)	39 (59.1)	
LCX	39 (26.0)	9 (13.6)	
RCA	63 (42.0)	18 (27.3)	
Lesion location			0.193
Proximal	62 (41.3)	36 (54.5)	
Mid	61 (40.7)	20 (30.3)	
Distal	27 (18.0)	10 (15.2)	
Anatomical severity			
Lesion length, mm	16.9 ± 7.0	19.2 ± 8.1	0.038
MLA, mm^2	3.02 ± 1.58	2.11 ± 1.43	<0.001
Diameter stenosis, %	43.1 ± 15.0	55.5 ± 15.4	<0.001
Distance from ostium, mm	47.8 ± 20.4	45.5 ± 27.2	0.489
Adverse plaque characteristics			
Low-plaque density	43 (28.7)	41 (62.1)	<0.001
Positive remodeling	16 (10.7)	23 (34.8)	<0.001
Napkin-ring sign	13 (8.7)	22 (33.3)	<0.001
Spotty calcification	31 (20.7)	28 (42.4)	0.001
Any adverse plaque characteristics*	63 (42.0)	53 (80.3)	<0.001
Hemodynamic parameters			
FFR_{CT}	0.79 ± 0.14	0.72 ± 0.17	0.006
ΔFFR_{CT}	0.06 ± 0.07	0.17 ± 0.17	<0.001
Wall shear stress, dyn/cm^2	145.5 ± 87.6	221.8 ± 113.2	<0.001
Axial plaque stress, dyn/cm^2	1,734.7 ± 1,896.8	2,585.9 ± 2,401.3	0.006

Values are n (%) or mean ± SD. *Plaques with any of low attenuation, positive remodeling, napkin-ring sign, or spotty calcification.

Abbreviations as in Table 1.

reclassification performance of each model was compared using relative integrated discrimination improvement (IDI) and category-free net reclassification index (NRI).

The prediction model was validated using 5-fold cross-validation with 1,000 random permutations of the patient population. Using this method, the distribution of area under the receiver operator characteristics curve (AUC) for incremental models from model 1 to model 3 was compared. In addition, an information gain attribute ranking technique was used to investigate the relative importance of each parameter. Parameters with a higher information gain value contribute more information to prediction models than ones with lower information gain (12). As a sensitivity analysis for the parameter ranking with respect to patient diversity, a bootstrapping technique based on 10,000 replicates was used. From 10,000 values of information gains, mean and 95% confidence interval (CI) were computed.

The risk for the culprit of subsequent ACS was compared on a per-lesion basis using Kaplan-Meier analysis, and hazard ratio (HR) with 95% CI was calculated using marginal Cox regression analysis.

RESULTS

BASELINE CHARACTERISTICS OF PATIENTS AND LESIONS. A total of 72 patients with ACS were included according to the enrollment and exclusion criteria as described in Figure 1, and 216 lesions (66 culprit and 150 nonculprit lesions) were included in the analysis. Although 78 culprit lesions were identified in coronary angiography from 72 patients, 12 culprit lesions were not defined in coronary CTA core lab because the radiologist was blinded to the rupture locations during the lesion definition process. In addition, 6 patients showed multiple culprit lesions in coronary angiography. Table 1 presents clinical and lesion characteristics. The median interval between coronary CTA and the occurrence of ACS was 338.0 days (interquartile range: 161.5 to 535.0 days). Ninety-three percent of patients presented with acute MI. The lesions were located at left main to left anterior descending (LAD) coronary artery, left circumflex artery, and right coronary artery in 40.3% (n = 87), 22.2% (n = 48), and 37.5% (n = 81), respectively. Mean values of %DS and FFR_{CT} were 46.9 ± 16.1% and 0.77 ± 0.15, respectively (Table 1).

COMPARISON OF ANATOMICAL SEVERITY, APC, AND HEMODYNAMIC PARAMETERS BETWEEN CULPRIT AND NONCULPRIT LESIONS. Compared with the nonculprit lesions, the culprit lesions of subsequent ACS were more frequently observed in the LAD (59.1% vs. 32.0%; $p < 0.001$) and had more severe stenosis (55.5 ± 15.4% vs. 43.1 ± 15.0%DS; $p < 0.001$) and longer lesion length (19.2 ± 8.1 mm vs. 16.9 ± 7.0 mm; $p = 0.038$) (Table 2). Regarding APC, culprit lesions showed a higher frequency of low-attenuation plaque, positive remodeling, napkin-ring sign, and spotty calcification than nonculprit lesions (all p values < 0.01). Regarding hemodynamic parameters, culprit lesions showed lower FFR_{CT} and higher $\triangle FFR_{CT}$, WSS, and axial plaque stress than nonculprit lesions (all p values < 0.01) (Table 2).

HEMODYNAMIC PARAMETERS AND THE RISK FOR THE CULPRIT OF SUBSEQUENT ACS. Figure 3 presents the Harrell's c-index, category-free NRI, and relative IDI values for the 3 models. Compared with model 1, model 2 showed higher discriminant ability (c-index 0.747 vs. 0.709; $p = 0.006$) as well as higher reclassification ability (NRI: 0.355, $p = 0.001$; relative IDI: 0.671; $p < 0.006$) in the identification of the culprit lesions for subsequent ACS. Model 3 showed further increase in discriminant ability (c-index 0.789 vs. 0.747; $p = 0.014$) and incremental reclassification ability (NRI: 0.287, $p = 0.047$; relative IDI: 0.368, $p < 0.001$), compared with model 2. The 5-fold

cross-validation with 1,000 random permutations of the patient population showed consistent improvement of AUC as adverse plaque and hemodynamic characteristics were added to the prediction model (Online Figure 4).

RISK FOR THE CULPRIT OF SUBSEQUENT ACS ACCORDING TO ADVERSE PLAQUE AND HEMODYNAMIC CHARACTERISTICS. When lesions were classified according to the presence of APC and AHC, the proportion of culprit lesions was highest in lesions with both APC and AHC (7.4%, 18.2%, and 51.1% for lesions with no APC/AHC, either APC or AHC, and both APC and AHC, respectively; $p < 0.001$) (**Figure 4A**). Lesions with both APC and AHC showed higher risk for the culprit of subsequent ACS than those with no APC/AHC (HR: 11.75; 95% CI: 2.85 to 48.51; $p = 0.001$) and with either APC or AHC (HR: 3.22; 95% CI: 1.86 to 5.55; $p < 0.001$) (**Figure 4B**).

PREDICTIVE MODELS WITH OTHER COMBINATIONS OF HEMODYNAMIC PARAMETERS. Table 3 shows the c-index and discrimination ability of various combination of hemodynamic parameters. Among 4 hemodynamic variables used in this study, $\triangle FFR_{CT}$ showed the highest c-index and incremental reclassification ability when added to model 2 as a single hemodynamic parameter (**Table 3**). Compared to model 2, discriminant ability (c-index 0.787 vs. 0.747; $p = 0.013$) and reclassification ability (NRI: 0.552, $p < 0.001$; relative IDI: 0.260, $p < 0.001$) were improved when $\triangle FFR_{CT}$ was added to model 2 (Online Figure 5). The 5-fold cross-validation results also showed consistent improvement of AUC with the addition of ΔFFR_{CT} to the prediction model (**Figure 5**). When the information gain of all included parameters was compared, $\triangle FFR_{CT}$ showed the highest rank (**Figure 6**). In addition, model 3 with resting hemodynamic parameters (resting Pd/Pa, △resting Pd/Pa, resting WSS, resting axial plaque stress) also showed significantly increased discriminant and reclassification ability compared with model 2 (Online Table 1). When upstream segmental values or peak values of WSS and axial plaque stress were used for model 3, the overall results were the same as the original ones (Online Table 2).

FIGURE 3 Comparison of Discriminant and Reclassification Ability of Predictive Models

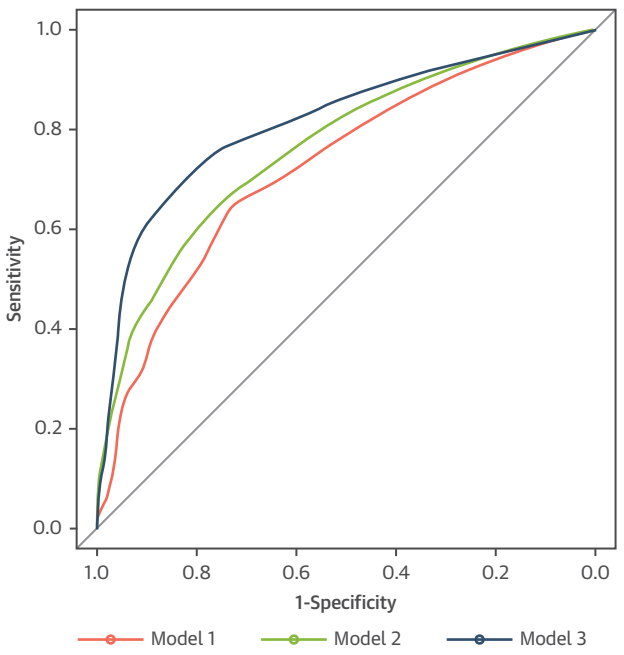

Prediction Model	C-index	Difference with previous model	P value	NRI	P value	IDI	P value
Model 1	0.709						
Model 2	0.747	0.038	0.006	0.355	0.001	0.671	<0.001
Model 3	0.789	0.025	0.014	0.287	0.047	0.368	<0.001

To determine incremental discriminatory and reclassification capacities of hemodynamic parameters in addition to anatomical severity and APC as predictors of ACS, 3 analytic models were constructed as follows: model 1: %DS and lesion length; model 2: model 1 + APC; model 3: model 2 + AHC. APC = adverse plaque characteristics; AHC = adverse hemodynamic characteristics; C-index = concordance statistic; IDI = relative integrated discrimination improvement; NRI = category-free net reclassification index; other abbreviations as in **Figures 1 and 2**.

DISCUSSION

The current study investigated the utility of noninvasive hemodynamic assessment using coronary CTA and CFD in the identification of high-risk plaque that caused subsequent ACS. The uniqueness of this study is that ACS was ascertained in all patients whose coronary lesions had been previously identified at coronary CTA. This allowed us to investigate the characteristics of lesions that would eventually be responsible for an acute event. The main findings are as follows. First, culprit lesions had a more severe degree of stenosis, longer lesion length, higher incidence of APC, and worse hemodynamic parameters (lower FFR_{CT}, higher $\triangle FFR_{CT}$, WSS, and axial plaque stress) than nonculprit lesions. Second, comprehensive assessment with anatomical stenosis severity, lesion length, APC, and AHC showed improved discriminatory and reclassification ability in the identification of the culprit for subsequent ACS compared with an anatomy-based model and APC-based model. The cross-validation with 1,000 random permutations also showed consistent results. Third, lesions with both APC and AHC showed

FIGURE 4 Proportion of Culprit Lesions and the Risk for Culprit Lesion on Acute Coronary Syndrome Among 3 Groups Classified by the Presence of Adverse Plaque and Hemodynamic Characteristics

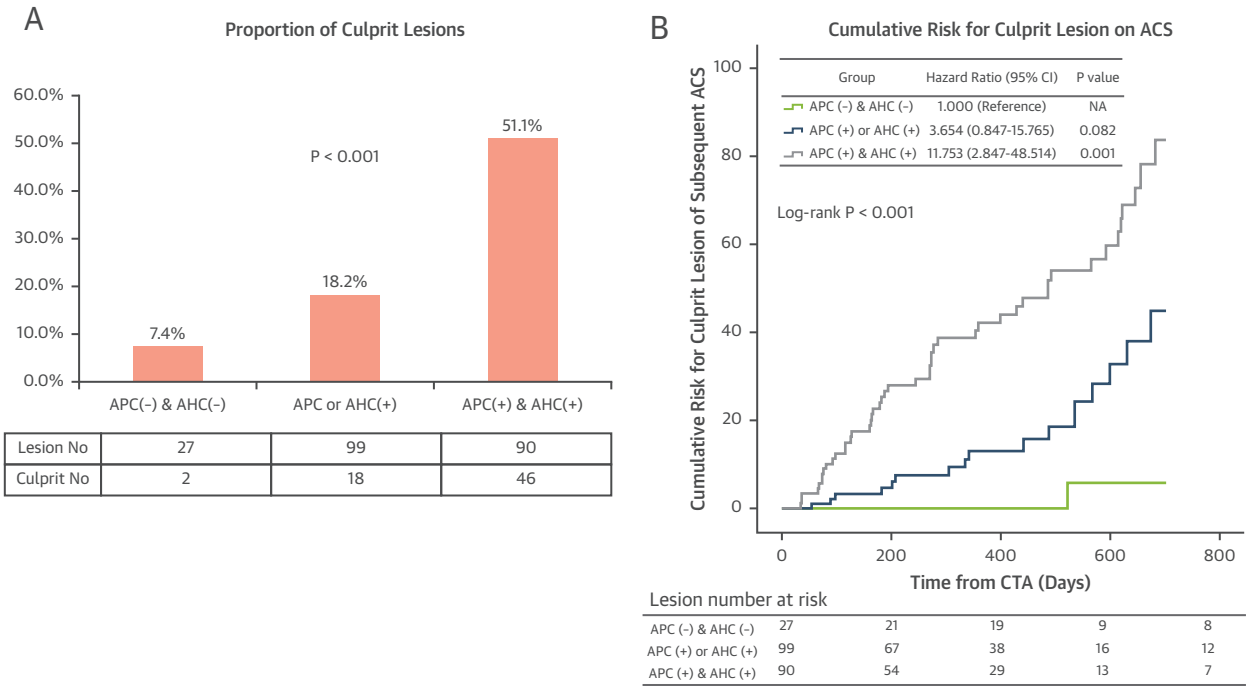

(A) All lesions were classified according to the presence of APC and AHC. The proportion of culprit lesions was significantly higher in lesions with both APC and AHC. **(B)** Lesions with both APC and AHC showed significantly higher risk compared with those with no APC/AHC and either APC or AHC. NA = not applicable; other abbreviations as in Figures 1 and 3.

TABLE 3 Comparison of C-Index Among Models With Various Combinations of Hemodynamic Parameters

Prediction Models	C-index	p Value*	NRI	p Value*	IDI	p Value*
Model 2 (%DS + Lesion length + APC)	0.747					
Model 2 + FFR_{CT}	0.775	0.570	0.105	0.455	0.087	0.210
Model 2 + APS	0.765	0.197	0.279	0.047	0.099	0.037
Model 2 + WSS	0.772	0.027	0.377	0.007	0.266	<0.001
Model 2 + ΔFFR_{CT}	0.787	0.031	0.552	<0.001	0.260	<0.001
Model 2 + FFR_{CT} + APS	0.781	0.445	0.180	0.210	0.176	0.043
Model 2 + FFR_{CT} + WSS	0.778	0.085	0.113	0.426	0.246	0.002
Model 2 + FFR_{CT} + ΔFFR_{CT}	0.790	0.053	0.336	0.018	0.240	0.006
Model 2 + APS + WSS	0.778	0.038	0.453	0.001	0.360	<0.001
Model 2 + APS + ΔFFR_{CT}	0.791	0.005	0.429	0.003	0.312	<0.001
Model 2 + WSS + ΔFFR_{CT}	0.786	0.006	0.435	0.002	0.333	<0.001
Model 2 + FFR_{CT} + WSS + ΔFFR_{CT}	0.789	0.021	0.344	0.016	0.304	<0.001
Model 2 + FFR_{CT} + WSS + APS	0.783	0.079	0.244	0.090	0.335	<0.001
Model 2 + FFR_{CT} + ΔFFR_{CT} + APS	0.793	0.041	0.274	0.057	0.289	0.002
Model 2 + WSS + ΔFFR_{CT} + APS	0.786	0.013	0.409	0.004	0.400	<0.001
Model 2 + FFR_{CT} + WSS + ΔFFR_{CT} + APS	0.789	0.014	0.287	0.047	0.368	<0.001

*The c-index, NRI, and relative IDI were compared with those of model 2.

APC = adverse plaque characteristics; APS = axial plaque stress; DS = diameter stenosis; IDI = integrated discrimination improvement; NRI = net reclassification index; WSS = wall shear stress; other abbreviation as in Table 2.

FIGURE 5 Comparison of Predictive Model With $\triangle FFR_{CT}$ Using 5-Fold Cross-Validation With 1,000 Random Permutation

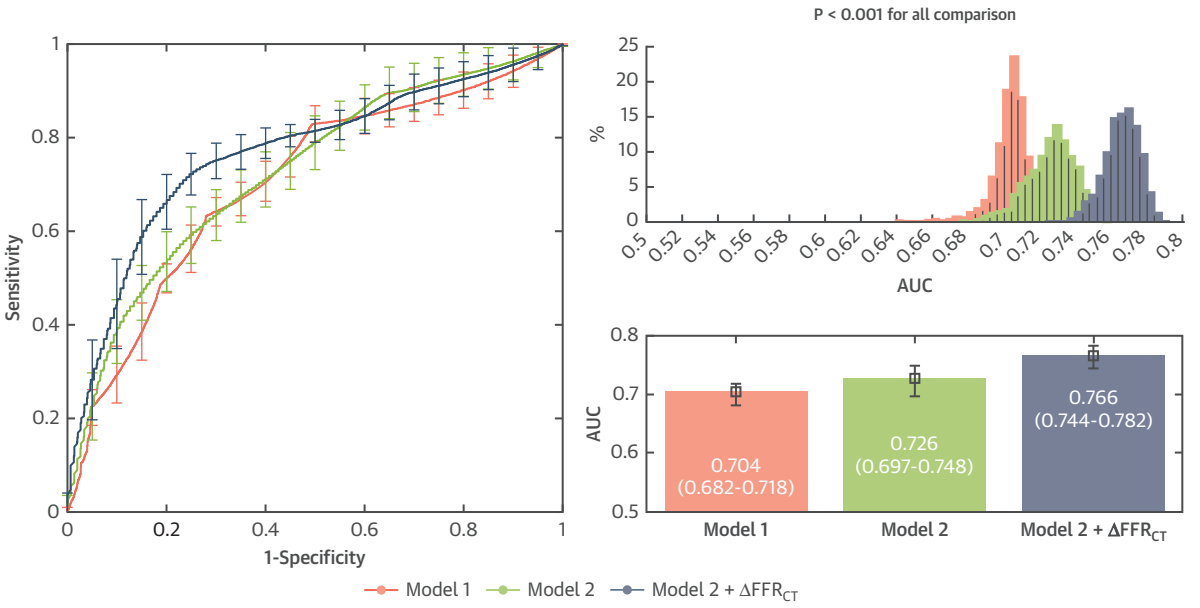

The 5-fold cross-validation using 1,000 random permutations of the patient population was performed to compare the AUC for incremental models from model 1: %DS + lesion length; model 2: model 1 + APC; model 3: model 2 + $\triangle FFR_{CT}$. The results also showed consistent improvement of AUC with the addition of ΔFFR_{CT} to the prediction model. AUC = area under the receiver operator characteristics curve; other abbreviations as in Figures 2 and 3.

significantly higher risk for the culprit of subsequent ACS than the other lesions.

PLAQUE VULNERABILITY AS A PREDICTOR OF ACS. Previous post-mortem studies provided insights on the morphology of atherosclerotic plaque prone to rupture and motivated the development of numerous noninvasive and invasive imaging techniques to detect vulnerable plaque. Invasive imaging studies consistently showed that the assessment of plaque characteristics could better predict the risk of cardiac events than the severity of lumen narrowing (2). Furthermore, noninvasive imaging studies based on coronary CTA also showed the added value of coronary CTA-derived APC and support the importance of assessing plaque characteristics in the prediction of future ACS risk (4,13). Our study also showed that the culprit lesions had more frequent APC than the nonculprit lesions and adding APC to anatomical stenosis severity improved discriminatory and reclassification ability in the identification of the culprit for subsequent ACS. Nevertheless, assessment of vulnerability based only on image features has some limitations, as the vulnerable plaques have a heterogeneous natural history and only a small proportion of them actually cause clinical events (2). In the study by Motoyama et al. (4), 83.7% of coronary CTA defined high-risk plaques did not cause any ACS events.

HEMODYNAMIC PARAMETERS AS A PREDICTOR OF ACS. Previous studies have suggested the potential role of biomechanical forces in plaque vulnerability and the development of ACS (3,14-17). Because plaques can rupture when the internal plaque stress exceeds the plaque strength (14), hemodynamic forces acting on the plaque can affect the risk of rupture, even among plaques with the same vulnerable features (6,15). Tanaka et al. (16) showed that the fibrous cap was thicker in culprit plaques with exertion-triggered ACS than in those with rest-onset ACS.

In the present study, we analyzed atherosclerotic lesions using coronary CTA scans performed before clearly documented ACS events (most were acute MI) to identify characteristics associated with culprit lesions for subsequent ACS. Culprit lesions showed higher %DS, longer lesion length, and higher frequency of APC than nonculprit lesions. In addition to those previously established predictors (4,8,13), the current study focused on assessing the role of noninvasively derived hemodynamic parameters. Culprit lesions showed significantly lower FFR_{CT} and higher magnitude of the other hemodynamic parameters ($\triangle FFR_{CT}$, WSS, and axial plaque stress) than

FIGURE 6 Comparison of Information Gain Among Included Parameters in Prediction Models

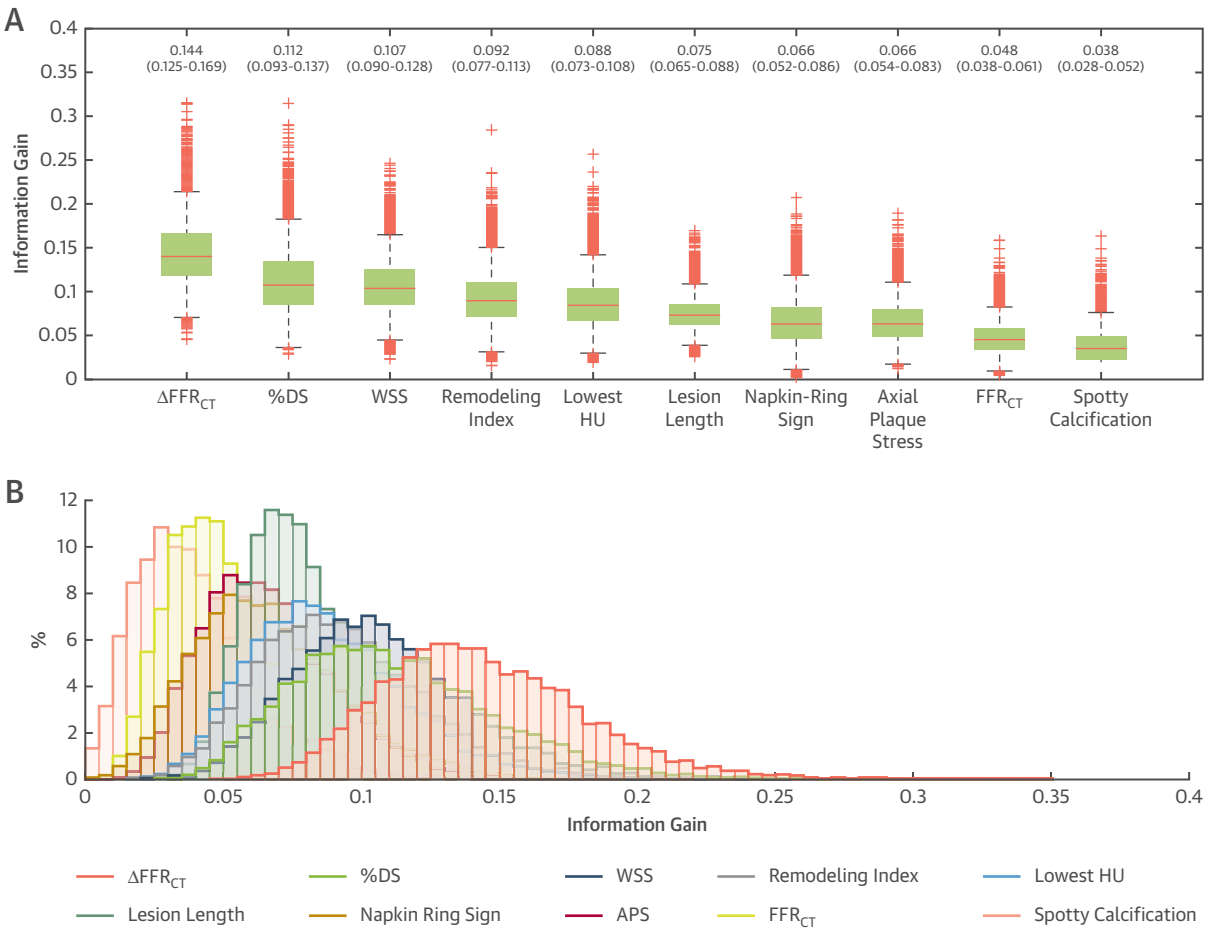

To investigate the relative importance of each parameter incorporated into models 1, 2, and 3, an information gain attribute ranking technique was used. **(A)** The median **(central marker)** and the 25th and 75th percentiles **(the bottom and top edges of the box)** of the information gain of each parameter. The **whiskers** extend to the most extreme data points not considered outliers, and the outliers are plotted individually using the "+" symbol. **(B)** The distribution of information gain of all the included parameters from bootstrapping analysis based on 10,000 replicates. HU = Hounsfield units; other abbreviations as in Figure 2.

nonculprit lesions. These results are intriguing because adverse hemodynamic features are present before the development of ACS. The addition of hemodynamic parameters to anatomical severity and APC improved the c-index and reclassification ability in the identification of high-risk plaque that caused ACS. The importance of hemodynamic parameters was also supported by significantly higher risk of subsequent ACS in lesions with both APC and AHC than the others. These results support the importance of integrating the 3 components—anatomical severity, APC, and AHC—to improve the accuracy of identifying high-risk plaques that can cause future ACS. Furthermore, because all the hemodynamic parameters introduced in the present study were derived using the same analysis as the FFR_{CT} computation, there would be no additional computational cost for adding hemodynamic parameter calculation beyond FFR_{CT}.

ROLE OF DIFFERENT HEMODYNAMIC PARAMETERS IN THE OCCURRENCE OF ACS. Among various hemodynamic parameters, our study focused on evaluating FFR_{CT}, ΔFFR_{CT}, WSS, and axial plaque stress, as previous studies showed the clinical relevance of these hemodynamic parameters (6,10,11,15,18,19). In the FAME (Fractional Flow Reverse Versus Angiography for Multivessel Evaluation) 2 study, among patients with low FFR (≤0.80), the group with deferred percutaneous coronary intervention exhibited a

significantly higher rate of clinical events than the group with percutaneous coronary intervention performed (18). FFR_{CT} has been shown to be a noninvasive means to estimate FFR and identify hemodynamically significant coronary stenosis (20). In addition, a large pressure drop across the lesion causes large net force acting on the plaque. In this respect, $\triangle FFR_{CT}$, a normalized pressure drop (i.e., pressure drop divided by aortic pressure), represents the force imbalance caused by the pressure drop. Because axial plaque stress is determined by both pressure and lesion geometry, this parameter can be different in lesions with the same ΔFFR according to the shape of lesion geometry, such as lesion length (6,10). WSS has been known to be associated with the initiation, growth, and vulnerable transformation of atherosclerotic plaques (11,15,17,19). Although previous studies focused on the relationship between low WSS and atherosclerosis, recent data suggest that high WSS above the physiologic range may also increase the risk of plaque rupture and platelet activity (7,19).

Although the combination of 4 hemodynamic parameters was used in the primary analysis of our study, it should be noted that the role of each hemodynamic parameter in the occurrence of ACS could be different, depending upon the characteristics of patients and lesions, as well as the time interval between coronary CTA and ACS event. In our study, a simpler combination of model 2 and $\triangle FFR_{CT}$ also showed significantly higher c-index (0.787 vs. 0.747) and reclassification ability (NRI: 0.553, IDI: 0.260) than model 2, and was as effective as the addition of all hemodynamic parameters (c-index: 0.787 vs. 0.789, NRI: 0.553 vs. 0.344, INI: 0.260 vs. 0.304). In addition, the information gain of $\triangle FFR_{CT}$ was the highest among the parameters evaluated in this study. This result implies that lesion-specific local hemodynamic parameters have more impact on plaque rupture and ACS than vessel-level hemodynamic parameters, such as FFR_{CT}. This simple model with $\triangle FFR_{CT}$ has the potential to be immediately used in real-world practice to discriminate ACS-prone lesions, as $\triangle FFR_{CT}$ can be easily calculated in the current FFR_{CT} algorithm. A further study is warranted to determine the best hemodynamic parameter, or its combinations, in diverse patient and lesion subsets.

STUDY LIMITATIONS. First, there was no control group per se in the current study. The current study compared APC and hemodynamic parameters between culprit and nonculprit lesions within the same patients. Because the risk of ACS is determined by numerous clinical characteristics of patients, using an internal control might reduce the influence of those confounding variables. Second, the present study used stenosis severity, lesion length, APC, and hemodynamic forces for the prediction of ACS risk. However, diverse factors, including cardiac contractility, pulse pressure, coronary spasm, endothelial dysfunction, interpatient variations in microcirculatory function, inflammation, and hematologic factors can also contribute to the development of ACS. In addition, the relatively long time span between coronary CTA and ACS events and inability to account for changes in medical treatment is another potential limitation of the current study. Third, the present study used steady-state hyperemic simulations for the calculation of main hemodynamic forces, and did not consider time-dependent fluid forces over the cardiac cycle, forces on the plaques due to cardiac contraction and relaxation, or the stresses within the plaques themselves. Fourth, although the current study focused on comprehensive assessment of anatomical severity, APC, and AHC, intraplaque stress was not used in our models. Fifth, the present study retrospectively collected coronary CTA data, obtained before the ACS event, and the number of patients was relatively small. Our results must be verified in a larger cohort including cost-effectiveness of the current approach. Based on the current study results, approximately 1,000 patients would be needed to conclusively validate the results. Sixth, the exclusion rate due to coronary CTA image quality was relatively high compared with previous studies. The current study adopted a high threshold for image quality to minimize the bias from coronary CTA image quality. The CFD core laboratory excluded 7 patients due to poor image quality. Among 27 patients excluded from the analysis by a coronary CTA core laboratory, 22 patients were excluded due to the lack of adequate raw data (13 due to absence of thin-slice computed tomographic [CT] data, 6 due to severe motion artifact, and 3 due to only perfusion CT data being available).

CONCLUSIONS

Noninvasive hemodynamic assessment enhanced the identification of high-risk plaques that subsequently caused ACS. The integration of noninvasive hemodynamic assessments may improve the identification of culprit lesions for future ACS.

ADDRESS FOR CORRESPONDENCE: Dr. Bon-Kwon Koo, Department of Internal Medicine and Cardiovascular Center, Seoul National University Hospital, 101 Daehang-ro, Chongno-gu, Seoul, 110-744, South Korea. E-mail: bkkoo@snu.ac.kr.

PERSPECTIVES

COMPETENCY IN MEDICAL KNOWLEDGE: Previous studies showed that the assessment of plaque composition such as thin fibrous cap, large lipid core, and active inflammation could better predict the risk of cardiovascular events than the severity of lumen narrowing. However, the vulnerable plaques have a heterogeneous natural history and only a small proportion actually causes clinical events.

COMPETENCY IN PATIENT CARE AND PROCEDURAL SKILLS: Because plaques can rupture when the internal plaque stress exceeds the plaque strength, hemodynamic forces acting on the plaque can affect the risk of rupture even among plaques with the same vulnerable features.

TRANSLATIONAL OUTLOOK 1: In the current study, we analyzed the atherosclerotic lesions on coronary CTA scans performed before ACS events to identify characteristics associated with subsequent ACS, and focused on the role of noninvasively derived hemodynamic parameters. The culprit lesions had a more severe degree of stenosis, longer lesion length, higher incidence of APC, and worse hemodynamic parameters than nonculprit lesions. The addition of hemodynamic parameters to anatomical severity, lesion length, and APC improved the c-index and reclassification ability in the prediction of ACS risk.

TRANSLATIONAL OUTLOOK 2: Our results suggest that the integration of noninvasive hemodynamic assessment would enhance the prediction ability for ACS risk and may help provide optimal treatment for those high-risk patients. Further study is warranted to determine the best hemodynamic parameter, or its combinations, in diverse patient and lesion subsets.

REFERENCES

1. Koskinas KC, Ughi GJ, Windecker S, Tearney GJ, Raber L. Intracoronary imaging of coronary atherosclerosis: validation for diagnosis, prognosis and treatment. Eur Heart J 2016;37:524–535a-c.

2. Stone GW, Maehara A, Lansky AJ, et al. A prospective natural-history study of coronary atherosclerosis. N Engl J Med 2011;364:226–35.

3. Maurovich-Horvat P, Ferencik M, Voros S, Merkely B, Hoffmann U. Comprehensive plaque assessment by coronary CT angiography. Nat Rev Cardiol 2014;11:390–402.

4. Motoyama S, Ito H, Sarai M, et al. Plaque characterization by coronary computed tomography angiography and the likelihood of acute coronary events in mid-term follow-up. J Am Coll Cardiol 2015;66:337–46.

5. Taylor CA, Fonte TA, Min JK. Computational fluid dynamics applied to cardiac computed tomography for noninvasive quantification of fractional flow reserve: scientific basis. J Am Coll Cardiol 2013;61:2233–41.

6. Choi G, Lee JM, Kim HJ, et al. Coronary artery axial plaque stress and its relationship with lesion geometry: application of computational fluid dynamics to coronary CT angiography. J Am Coll Cardiol Img 2015;8:1156–66.

7. Park JB, Choi G, Chun EJ, et al. Computational fluid dynamic measures of wall shear stress are related to coronary lesion characteristics. Heart 2016;102:1655–61.

8. Bentzon JF, Otsuka F, Virmani R, Falk E. Mechanisms of plaque formation and rupture. Circ Res 2014;114:1852–66.

9. Roffi M, Patrono C, Collet JP, et al. 2015 ESC guidelines for the management of acute coronary syndromes in patients presenting without persistent ST-segment elevation: Task Force for the Management of Acute Coronary Syndromes in Patients Presenting without Persistent ST-Segment Elevation of the European Society of Cardiology (ESC). Eur Heart J 2016;37:267–315.

10. Lee JM, Choi G, Hwang D, et al. Impact of longitudinal lesion geometry on location of plaque rupture and clinical presentations. J Am Coll Cardiol Img 2017;10:677–88.

11. Samady H, Eshtehardi P, McDaniel MC, et al. Coronary artery wall shear stress is associated with progression and transformation of atherosclerotic plaque and arterial remodeling in patients with coronary artery disease. Circulation 2011;124:779–88.

12. Hall MA, Holmes G. Benchmarking attribute selection techniques for discrete class data mining. IEEE Trans Knowl Data Eng 2003;15:1437–47.

13. Puchner SB, Liu T, Mayrhofer T, et al. High-risk plaque detected on coronary CT angiography predicts acute coronary syndromes independent of significant stenosis in acute chest pain: results from the ROMICAT-II trial. J Am Coll Cardiol 2014;64:684–92.

14. Brown AJ, Teng Z, Calvert PA, et al. Plaque structural stress estimations improve prediction of future major adverse cardiovascular events after intracoronary imaging. Circ Cardiovasc Imaging 2016;9:e004172.

15. Kwak BR, Back M, Bochaton-Piallat ML, et al. Biomechanical factors in atherosclerosis: mechanisms and clinical implications. Eur Heart J 2014;35:3013–20.

16. Tanaka A, Imanishi T, Kitabata H, et al. Morphology of exertion-triggered plaque rupture in patients with acute coronary syndrome: an optical coherence tomography study. Circulation 2008;118:2368–73.

17. Stone PH, Saito S, Takahashi S, et al. Prediction of progression of coronary artery disease and clinical outcomes using vascular profiling of endothelial shear stress and arterial plaque characteristics: the PREDICTION Study. Circulation 2012;126:172–81.

18. De Bruyne B, Fearon WF, Pijls NH, et al. Fractional flow reserve-guided PCI for stable coronary artery disease. N Engl J Med 2014;371:1208–17.

19. Fukumoto Y, Hiro T, Fujii T, et al. Localized elevation of shear stress is related to coronary plaque rupture: a 3-dimensional intravascular ultrasound study with in-vivo color mapping of shear stress distribution. J Am Coll Cardiol 2008;51:645–50.

20. Nørgaard BL, Leipsic J, Gaur S, et al. Diagnostic performance of noninvasive fractional flow reserve derived from coronary computed tomography angiography in suspected coronary artery disease: the NXT trial (Analysis of Coronary Blood Flow Using CT Angiography: Next Steps). J Am Coll Cardiol 2014;63:1145–55.

KEY WORDS acute coronary syndrome, adverse plaque characteristics, axial plaque stress, computational fluid dynamics, coronary computed tomography angiography, coronary plaque, wall shear stress

APPENDIX For supplemental text, figures, tables, and a reference, please see the online version of this paper.